Supplementary information

Construction of efficient Pb(II) carboxylate catalysts for Oxygen and Hydrogen Evolution Reactions

Janak,[a] Vijay S. Sapner[b,c], Bhaskar R. Sathe*[c] and Sadhika Khullar*[a]

[a]Department of Chemistry, Dr. B.R. Ambedkar National Institute of Technology Jalandhar, GT Road by pass Jalandhar, Punjab-144008, India
[b]Department of Chemistry, Shri Mathuradas Mohota College of Science, Nagpur, Maharashtra - 440024, India
[c]Department of Chemistry, Dr. Babasaheb Ambedkar Marathwada University, Ch. Sambhaji Nagar, Aurangabad, Maharashtra - 431001, India

Corresponding author email: khullars@nitj.ac.in, bhaskarsathe@gmail.com

Contents

Materials and Physical Measurements

All chemicals and solvents were obtained from commercial sources included with analytical grade and utilized without any additional purification. TPBN ligand was prepared at ambient conditions following the literature method.

Proton (^{1}H) NMR data of ligand was recorded in $CDCl_3$ at 25 °C with the help of Bruker ARX-400 spectrometer from IISER Mohali, where chemical shifts are described with respect to the enduring solvent peaks.

Elemental analysis (C, H, N) was carried out on a Perkin Elmer analyzer from IISER Kolkata.

ATR spectra were captured in the range of 4000−650 cm^{-1} by using a Bruker Alpha **II** Germany ATIR Spectrometer at NIT Jalandhar.

The molecular Hirshfeld surfaces[S1] within crystal structures were constructed by considering the electron distribution calculated as the sum of the spherical atom electron densities. The normalized contact distance (d_{norm}) is based on both de (the distance from the point to the nearest nucleus external to the surface) and di (the distance to the nearest nucleus internal to the surface) and r_i^{vdw} and r_e^{vdw} are the internal and external van der Waals (vdW) radii, is calculated by the equation. The 2D fingerprint plot[S2] provides a comprehensive representation of all intermolecular contacts present within the crystal structures. Both Hirshfeld surfaces and the 2D fingerprint plots were generated using the Crystal Explorer[S3] program.

Gas absorption Studies for each measurement 100 mg of 1 was placed in an analysis tube to do pretreatment at 120 °C for 12-24 h (depending on the gas/vapor type). Data were collected in a BELSORP Max instrument (IIT delhi) with warm and cold free-space (dead volume) correction measurements for all isotherms.

Thermogravimetric analysis (TGA) was recorded under dinitrogen from 25 to 500 °C at a fixed heating rate of 10 °C/min on a Shimadzu DTG-60H instrument from IISER Mohali.

Powder X-ray Studies were measured using a Rigaku Ultima IV diffractometer across a 2 range of 5-50° and using a mortar and pestle, each sample was made into a fine powder and put on a glass sample holder for room temperature measurement at a scanning speed of 2.8° per minute and a 0.02° step.

Single crystal data collection and refinements. The crystal of **CP1** which was grown by layering method, was transferred from the mother liquor to the mineral oil for manipulation, selection and mounting. One of the crystals with a bright shine was chosen, examined under an optical microscope, and then placed within the nylon loop on the goniometer head after that it was subjected to a cold stream of nitrogen gas for gradual cooling to a temperature of 100 K. The Burker Kappa APEX II diffractometer equipped with a CCD detector with a fixed distance of crystal to detector at 60 mm and sealed-tube monochromated Mo Kα radiation was used to perform the initial crystal evolution and data collection by using the program APEX2.[S3] The diffractometer was interfaced to a PC with APEX2[S4] program installed in it that controlled the crystal centering, unit cell determination, refinement of the cell parameters and data collection. Using the SAINT[S4] software, the integration of data, fitting of reflection profiles, and values of F2 and σ(F2) for each reflection were obtained. Data were also corrected for Lorentz and polarization effects. The subroutine XPREP[S5] was used for the processing of data that included determination of space group, application of an absorption correction (SADABS)[S4], merging of data and generation of files necessary for solution and refinement. The crystal structures were solved and refined by using SHELXL 2014.[S6] Several full-matrix least-squares/difference Fourier cycles were performed, locating the remainder of the non-hydrogen atoms and to have reasonable thermal parameters and converged refinement resulting in the lowest residual factors and optimum goodness of fit. Final crystallographic parameters and basic information pertaining to data collection and structure refinement are summarized in Table 1. All crystallographic Fig. were drawn using Mercury V (8.0) TOPOS Pro softwares.

Contact angle measurements (determination of CA, CAH) was performed using the instrument drop shape analyzer, DSA25 S (Kruss, Germany). The software-controlled dosing system was used to cast liquid drops on a flat surface at ambient condition (25 °C, 45–50 % relative humidity) for determination of CAs. The images of the drops were recorded by CCD (charged coupled device) camera attached to the instrument. The inbuilt Young Laplace fitting method in the ADVANCE software was used for image analysis and determination of CAs. Standard deviations in the CA measurements were ± 2°. The top or side view drop motion or images were recorded by 25 MP canon camera (EOS M200 w/EFM15-45 kit lens).

Field Emission Scanning Electron Microscopy (FESEM) experiments including **Energy dispersive X-ray (EDX)** of metal complexes were carried out on an EVO/SIGMA instrument at NIT Jalandhar**. High Resolution Transmission Electron Microscopy (HRTEM)** was performed on FEI Tecnai G2 F20 equipped with a field emission gun

operated at 200 Kv with 1 mg sample well dispersed in ethanol (10 mL) using a sonicator for 20 minutes and then put on the copper grid, which was allowed to dry using a lamp for 30 minutes. SEAD pattern were draw through Image J software.

X-ray Absorption Spectroscopy (XPS) analysis were carried out with a Al Kα a monochromatic Source on an model AXIS Supra of Karos Analytical Ltd at IIT Delhi.

Electrochemical Measurements All electrochemical experiments were carried out with a three-electrode setup on a Metrohum Autolab PGSTAT302N electrochemical workstation from the Netherlands. A glassy carbon electrode (GCE, 3 mm in diameter), saturated calomel electrode, and platinum foil were used as working, reference, and counter electrodes, respectively. GCE was polished using 1 μm, 0.3 μm, and 0.05 μm Al_2O_3 powders, then subjected to ultrasonication in deionized water and ethanol for 5 min each. The catalyst ink for the working electrode can be made by dispersing 5mg of catalyst in a solvent comprising a 100:1 isopropanol nafion (5 wt%) solution and then sonicated for 60 min. to make a homogenous ink. The resulting homogeneous solution was loaded on cleaned GCE using the drop-casting method and then dried at room temperature. The electrocatalytic studies towards HER and OER were carried out using CV, LSV, and EIS at a 50 mV/s scan rate in 1 M H_2SO_4 and 1 M KOH solution. The potential was converted using $E_{RHE} = E_{SCE} + 0.244V + 0.0591*pH$. Tafel plots are generated using a forward scan of LSV curves at a scan rate of 50 mV/sec using the Tafel equation ($\eta = b \times \log j + a$, where η is the overpotential, j is the current density, and b is the Tafel slope).

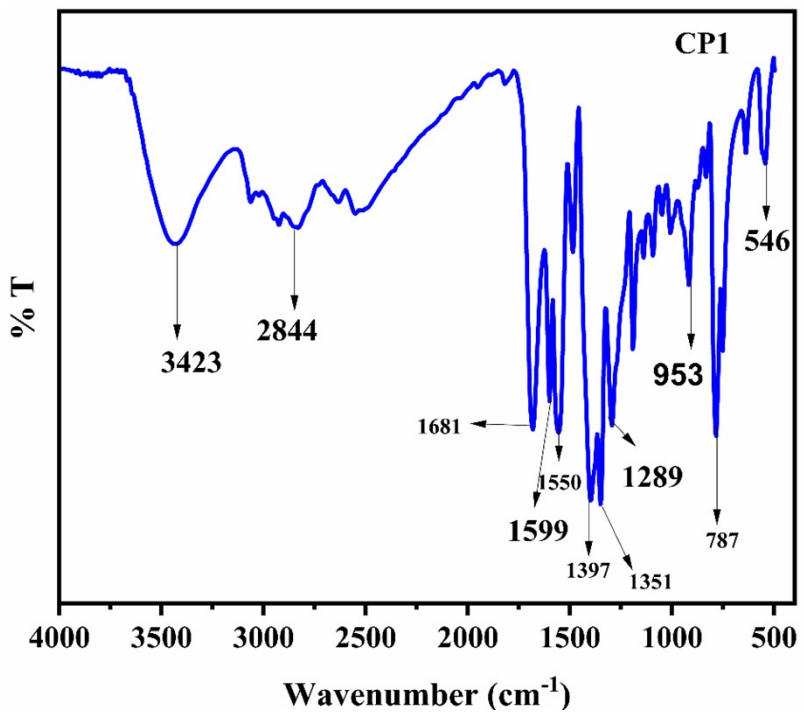

Fig. S1 FTIR spectrum of **CP1**.

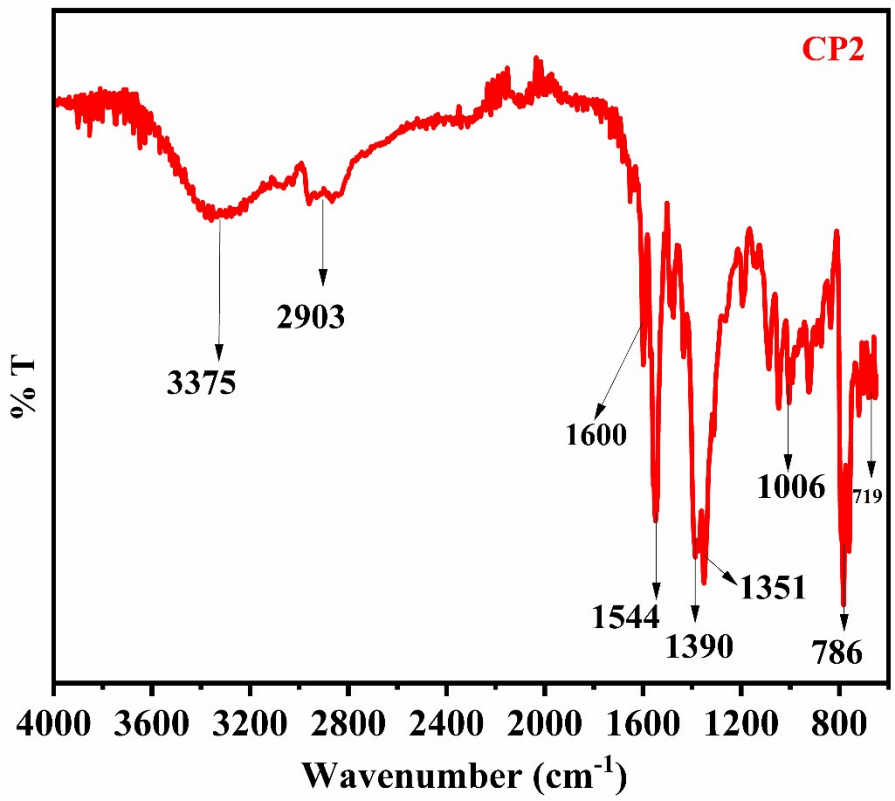

Fig. S2 FTTR spectrum of **CP2**.

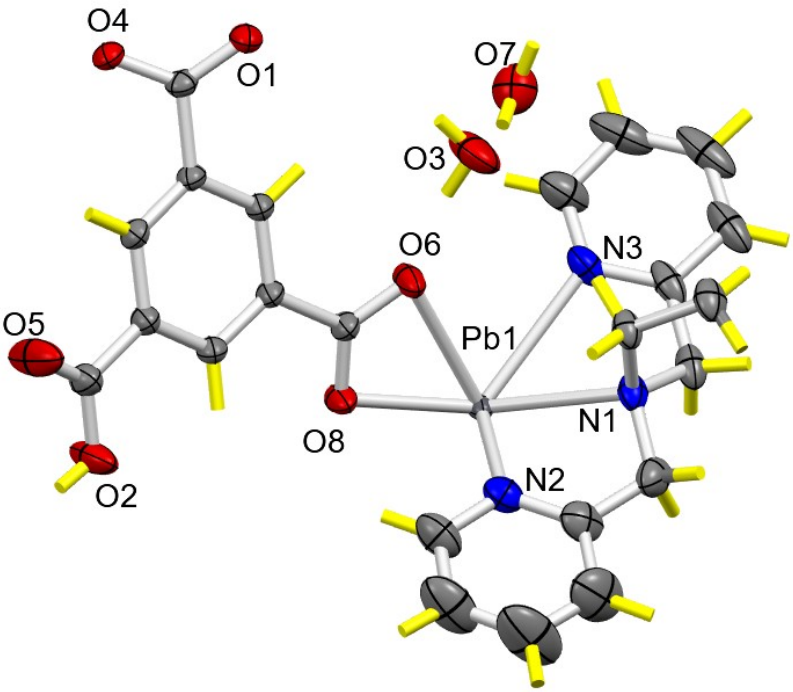

Fig. S3 Labelled asymmetric unit of **CP1**.

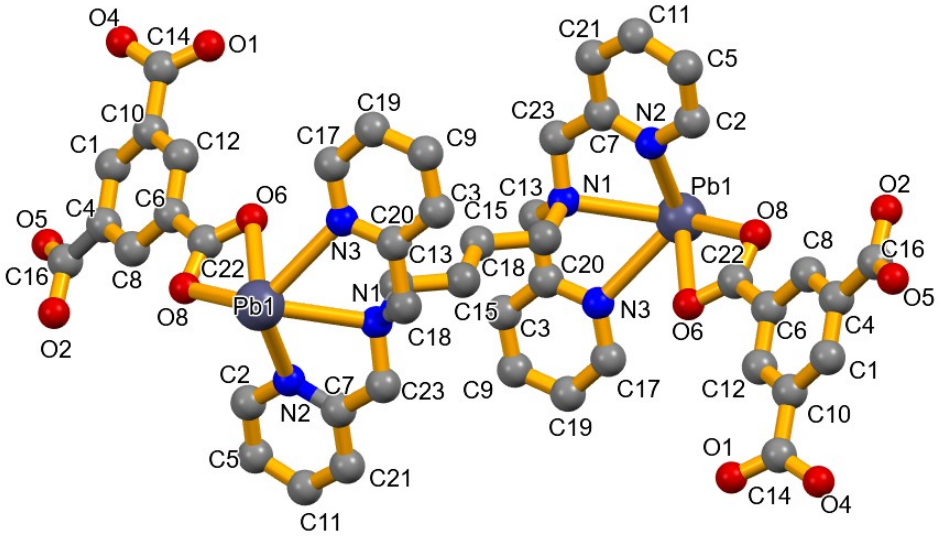

Fig. S4 Labelled and schematic representation of **CP1**.

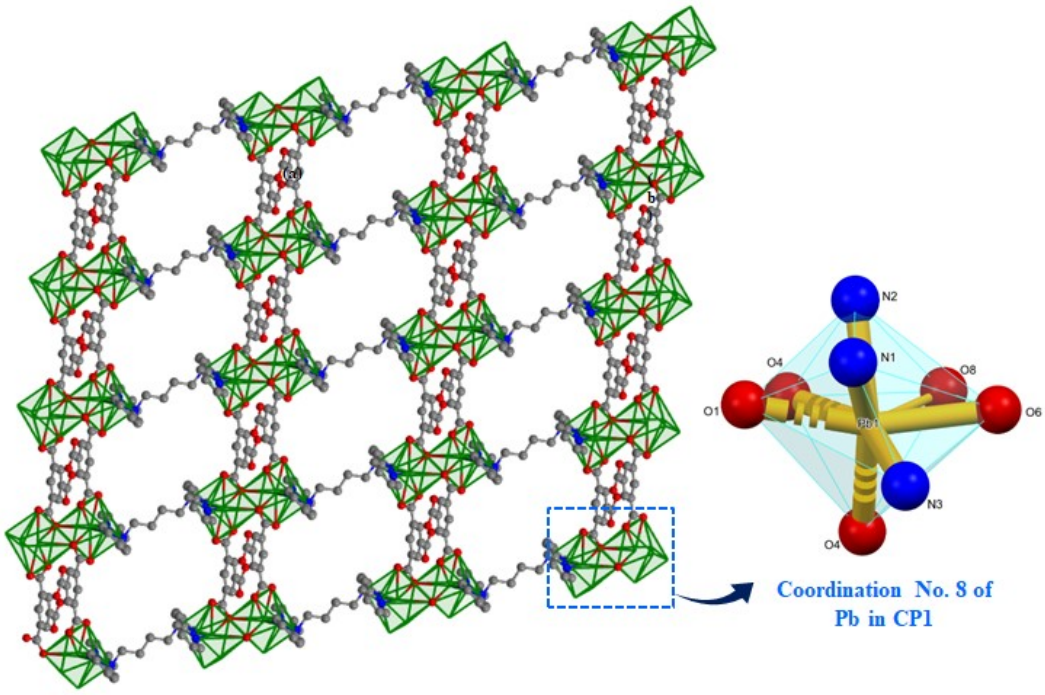

Fig. S5 (a) 2D polymeric structure of **CP1** with the polyhedral view, Color codes: dark gray, Pb; gray, C; blue, N; red, O. **(b)** mono-capped distorted pentagonal pyramidal geometry representation around Pb(II) centre in **CP1**.

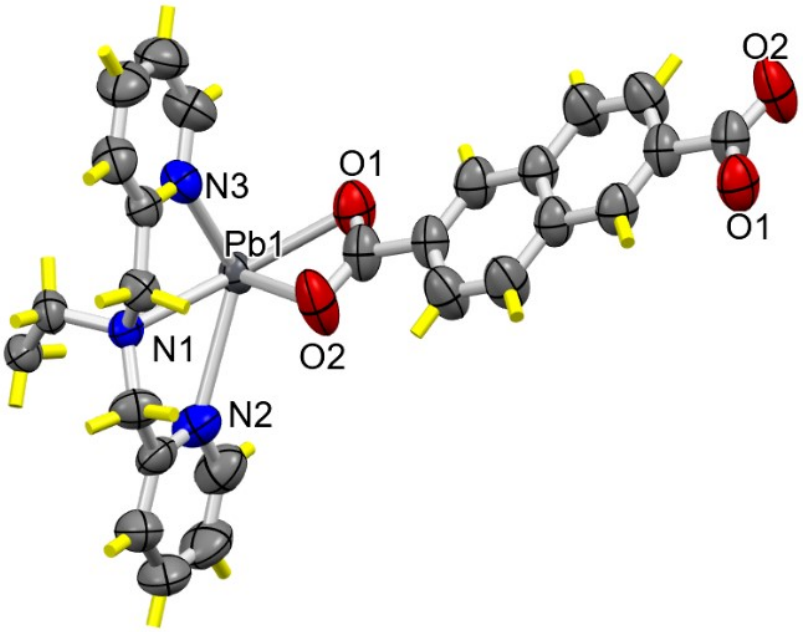

Fig. S6 Labelled asymmetric unit of **CP2**.

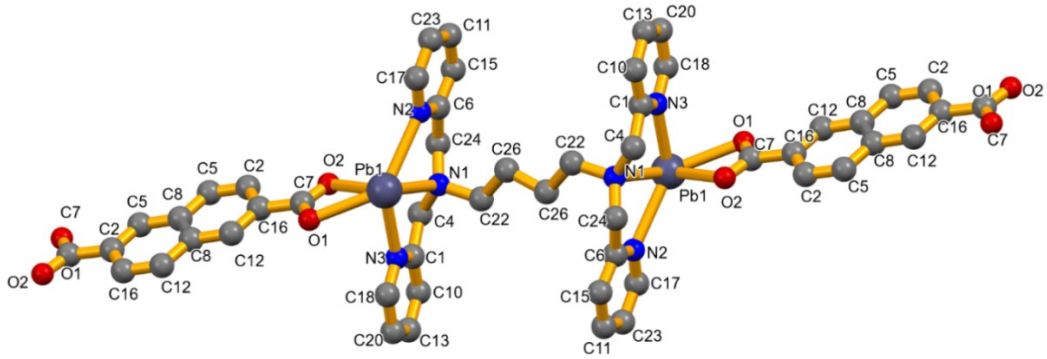

Fig. S7 Labelled and schematic representation of **CP1**.

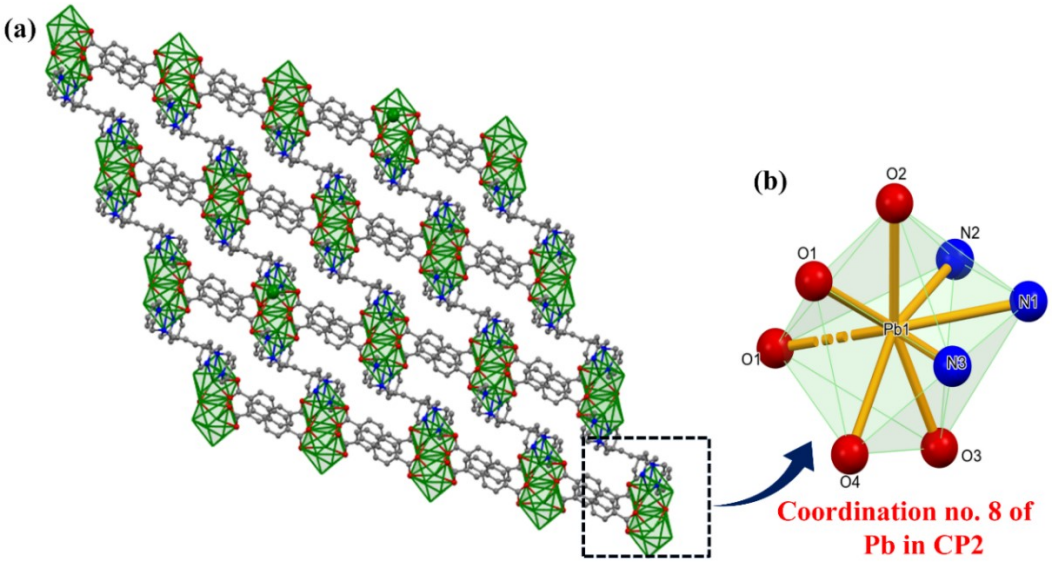

Fig. S8 (a) 2D polymeric structure of **CP2** with the polyhedral view, Color codes: dark gray, Pb; gray, C; blue, N; red, O. **(b)** mono-capped distorted pentagonal pyramidal geometry representation around Pb(II) centre in **CP2**.

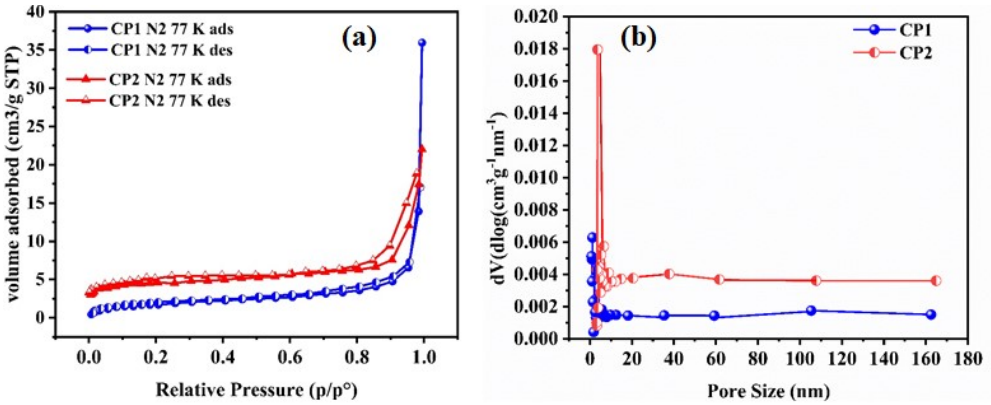

Fig. S9 BET Data **(a)** N_2 gas adsorption-desorption curves for **CP1** and **CP2** at 77 K, and (b) Distribution Pore size curve of **CP1** and **CP2**.

Table S1. BET Surface area, Pore Size and Pore volume of **CP1** and **CP2**.

Sample Name	BET Surface area / (m^2/g)	Pore size / (nm)	Pore Volume / (cm^3/g)
CP1	7.29	8.296	1.75
CP2	10.01	7.258	2.236

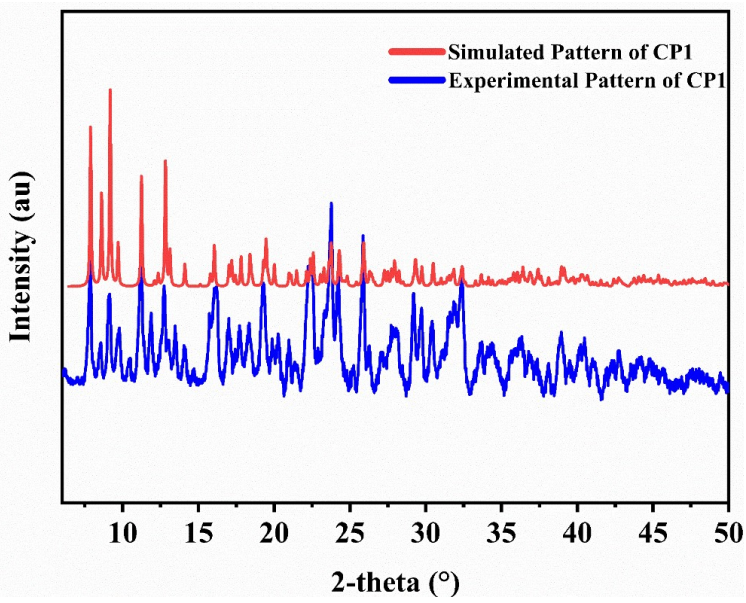

Fig. S10 Experimental and Simulated Powder X-ray scan of **CP1.**

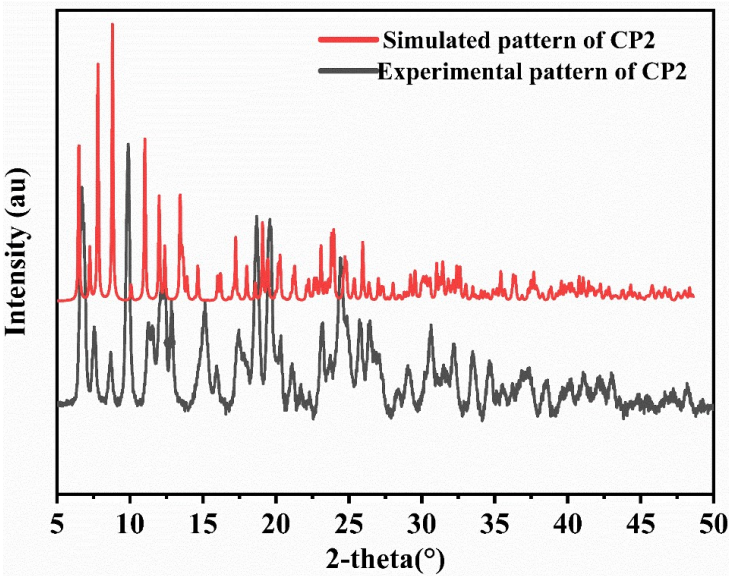

Fig. S11 Experimental and Simulated Powder X-ray scan of **CP2.**

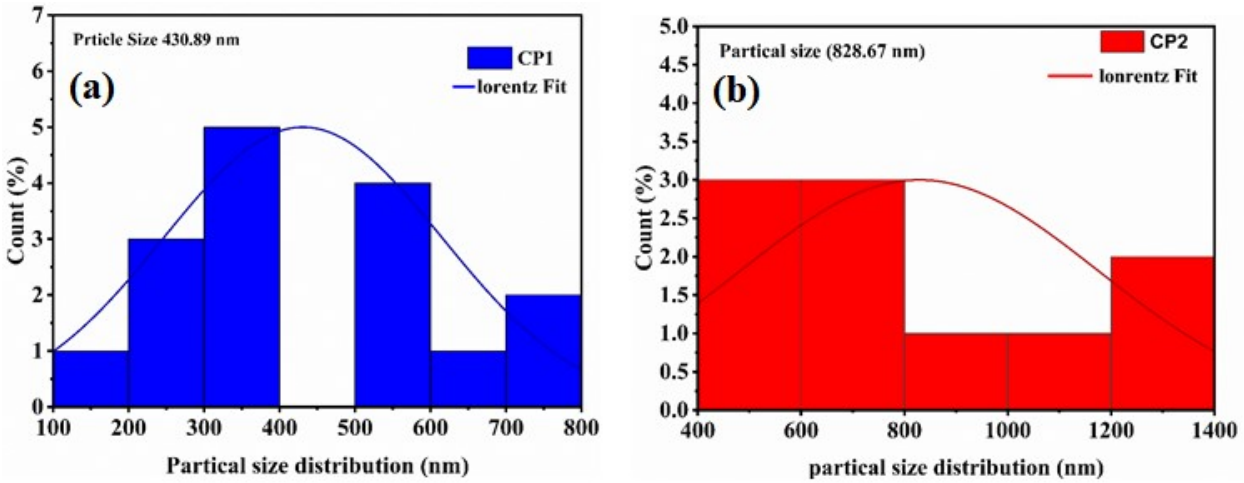

Fig. S12 Average particle size distribution of (a) **CP1** and (b) **CP2.**

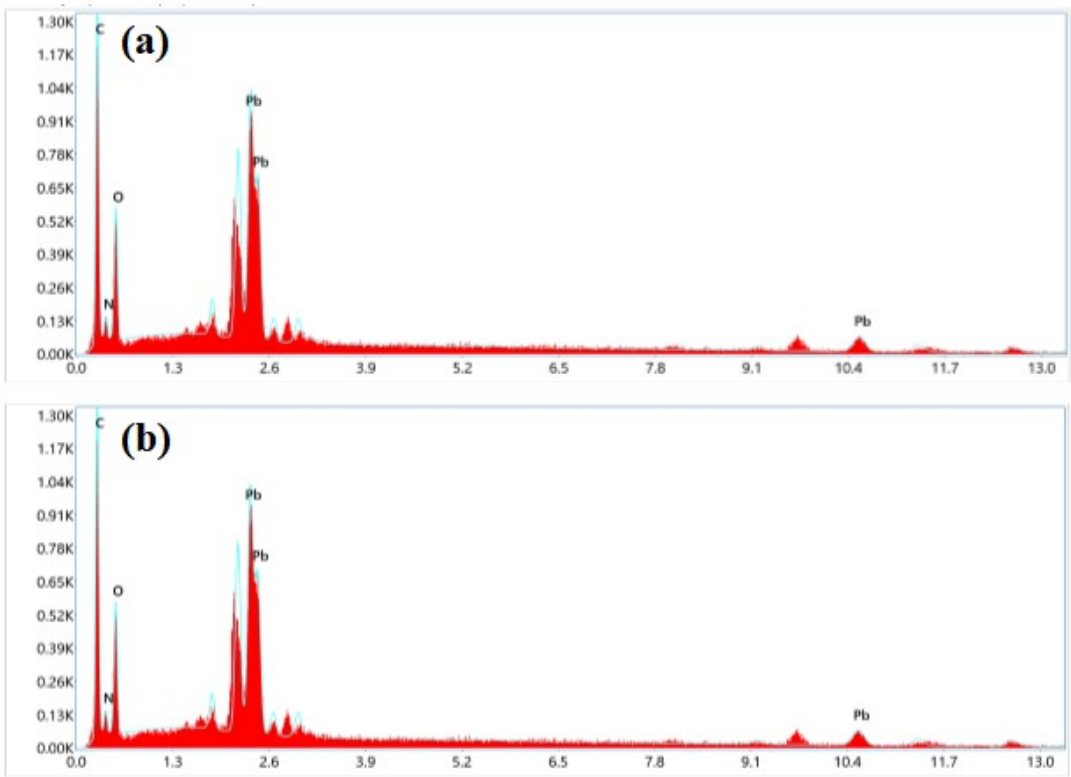

Fig. S13 EDX Spectrum of (a) **CP1** and (b) **CP2.**

Table S2. Selected bond lengths (Å) and bond angles (°) in CP1.

Bond lengths (Å)

Pb1	O1	2.6493	Pb1	Pb1 (in core structure)	4.512
Pb1	O4	2.6296	Pb1	Pb1 (separated by TPBN)	10.899
Pb1	O6	2.7349	Pb1	Pb1(separated by BTC)	10.348
Pb1	O8	2.4869	C15	C18	2.518
Pb1	N1	2.7306	O1	O6	5.023
Pb1	N2	2.597	O4	O8	7.071
Pb1	N3	2.842	C22	C14	5.014

[1]+X,-1+Y,+Z; [2]-X,-Y,1-Z

Bond angles (Å)

O1[1]	Pb1	O6	163.89(7)	O8 Pb1 O6	49.40(5)
O1[1]	Pb1	N1	76.48(6)	O8 Pb1 N1	124.93(7)
O1[1]	Pb1	N3	107.39(7)	O8 Pb1 N2	76.99(8)
O4[1]	Pb1	O1[1]	49.67(5)	O8 Pb1 N3	124.53(7)
O4[1]	Pb1	O6	129.46(5)	N1 Pb1 O6	92.92(6)
O4[1]	Pb1	N1	116.50(6)	N1 Pb1 N3	59.88(7)
O4[1]	Pb1	N3	153.37(7)	N2 Pb1 O1[1]	74.67(7)
O6	Pb1	N3	76.55(7)	N2 Pb1 O4[1]	71.89(6)
O8	Pb1	O1[1]	127.94(5)	N2 Pb1 O6	89.73(8)
O8	Pb1	O4[1]	80.32(5)	N2 Pb1 N1	62.41(7)
O8	Pb1	O6	49.40(5)	N2 Pb1 N3	119.44(7)

[1]+X,-1+Y,+Z; [2]+X,1+Y,+Z; [3]-X,-Y,1-Z

Table S3. Selected bond lengths (Å) and bond angles (°) in CP2.

Pb1	O1	2.621(2)	Pb1	Pb1 (in core structure)	4.081
Pb1	O3	2.531(2)	Pb1	Pb1 (separated by TPBN)	9.340
Pb1	O2	2.761(2)	Pb1	Pb1(separated by NDC)	13.727
Pb1	O4	2.586(2)	C22	C26	2.505
Pb1	N1	2.773(2)	O1	O4	9.051
Pb1	N2	2.861(3)	O2	O3	7.071
Pb1	N3	2.558(2)	C14	C19	8.002

Bond lengths (Å)

[1]1-X,1-Y,2-Z; [2]2-X,1-Y,-Z; [3]1-X,2-Y,-Z

Bond angles(Å)

O1 Pb1 N1	121.92(6)	O4 Pb1 N2	136.34(7)
O1 Pb1 N2	131.84(7)	N1 Pb1 N2	60.97(7)
O3 Pb1 O1	136.75(8)	N3 Pb1 O1	77.60(7)
O3 Pb1 O4	51.20(7)	N3 Pb1 O4	74.57(7)
O3 Pb1 N1	79.21(7)	N3 Pb1 N1	64.71(7)
O3 Pb1 N2	91.14(8)	N3 Pb1 N2	125.66(7)
O3 Pb1 N3	80.09(8)	O4 Pb1 O1	87.11(7)
O4 Pb1 O1	87.11(7)	O4 Pb1 N1	120.14(7)

[1]1-X,1-Y,2-Z; [2]2-X,1-Y,-Z; [3]1-X,2-Y,-Z

Electrochemical studies. The electrocatalytic study of **CP1** and **CP2** was carried out by using a three-electrode setup where Ag/AgCl as a reference electrode, Pt-wire as a counter electrode, and carbon glassy electrode (GCE) was used as a working electrode in both 1M H_2SO_4 and 1M KOH (used as an electrolyte) aqueous solution at room temperature.

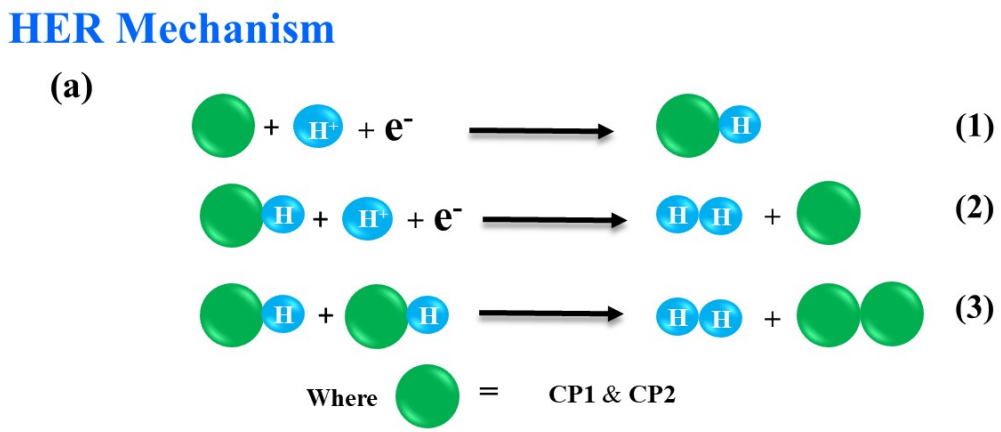

Fig. S14 Mechanism for HER in acidic medium by Heyrovsky, Volmer and Tafel. Where stands for the **CP1** and **CP2** as an electrocatalyst for water-splitting reactions via HER.

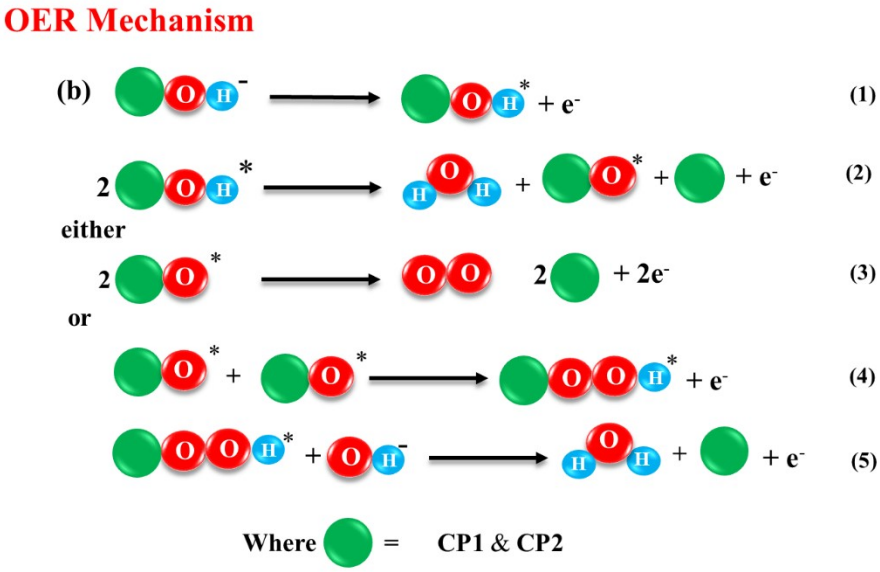

Fig. S15 Mechanism for OER in alkaline medium. Where stands for the **CP1** and **CP2** as an electrocatalyst for water-splitting reactions via OER

Electrochemically active surface area (ECSA) Calculations:

The electrochemical double-layer capacitance (Cdl) of the electrocatalysts in 1.0 M KOH for OER and 1.0 M H_2SO_4 were assessed by employing cyclic voltammetry (CV) in a non-Faradaic zone at various scan rates of 20, 40, 60, 80 and 100 mV/s respectively, in order to quantify the Electrochemical active surface area (ESCA) of the **CP1** and **CP2** as an electrocatalysts as shown in Fig. 12. The cyclic voltammograms (CVs) of catalysts measured in the region of 1.27 V to 1.323 V, where the current response should be only owing to the charging of the double layer. They plotted the capacitive currents against the scan rate and used Equation (S1) to determine charge double layer capacitance (C_{dl}), where the values of C_{dl} for **CP1** and **CP2** are 1.22 mF/cm^{2}and 1.95 mF/cm^{2}for OER and 87.5 μF/cm^{2}and 435 μF/cm^2 for HER plotted the capacitive currents against the scan rate and used Equation (1) to determine C_{dl}

$$C_{dl} = \frac{(\text{Anodic slope - cathodic slope})}{2} \quad \text{(S1)}$$

And the Specific Capacitance (Cs) also determined the equation (S2)

$$C_s = \frac{A}{2\Delta V mk} \quad \text{(S2)}$$

Where, Cs= Specific Capacitance in F/g

A= absolute area inside the CV, m = mass of active materials, k = scan rate (V/s) $\Delta V = (V_2 - V_1)$ = Potential window

By dividing equation (S1) and (S2) Electrochemically active surface area (ECSA) can calculate as follows:

$$ECSA = \frac{Cdl}{Cs} \quad (S3)$$

Where Cs is the specific capacitance and Cdl is the Electrochemical double-layer capacitance

The ESCA values for **CP1** and **CP2** for both HER and OER are mentioned below

ECSA = 0.014 cm^2 for **CP1** for HER

ECSA = 0.059 cm^2 for **CP2** for HER

ECSA = 0.052 cm^2 of **CP1** for OER

ECSA = 0.053 cm^2 of **CP2** for OER

We also calculated the roughness factor (RF) of **CP1** and **CP2** for both HER and OER. The following equation (S4) was applied to calculate RF:

$$RF = ECSA/A_g \quad (S4)$$

Where Ag = 0.071 cm^2 is the geometric area of the glassy carbon electrode. The RF values of **CP1** and **CP2** for HER and OER as 0.197, 0.831, 0.073 and 0.074 respectively.

Turnover frequency (TOF): The turnover frequency as the H_2 or O_2 molecules per site per seconds (S9) (per **CP1** and **CP2** site) was calculated by assuming 100% faradaic efficiency with the following equation (S5):

$$TOF = \frac{j}{(nFm)} \quad (S5)$$

Where, j = the current density (mA/cm^2); n= no. of electron in both HER and OER, F= Faraday constant; m = the number of moles in catalyst.

The TOF values of **CP1** and **CP2** as 1.05 s^{-1} and 3.21 s^{-1} for OER and 1.97 s^{-1} and 9.65 s^{-1} respectively, for HER.

Number of catalytic active sites

By determining the number of active catalytic sites of electrocatalysts using the redox peak method,[95] the electrochemical and catalytic behavior of **CP1** and **CP2** were studied. The Pb^{2+}/Pb^{3+} redox reaction is responsible for an extra electron-transfer process at roughly 1.53V, and 1.49 V vs RHE for **CP1** and **CP2** respectively.

However, the charge associated with the resulting PbOOH is calculated from eqn (S6) using the oxidation peak area from Figure S22 (a and b).

$$\text{Charge Associated with Oxidation Peak} = \frac{Oxidation\ Peak\ Area}{\text{Scan Rate}} \quad (S6)$$

The following equation (S7)[96] could be used to determine the total number of active sites created on the electrocatalytic surface,

$$\text{Number of Active Sites } (\Gamma) = \frac{\text{Charge Associated with Oxidation Peak}}{\text{N} \times \text{Charge of Electron}} \quad \text{(S7)}$$

Where, Γ is the number of active sites, and N is the number of electrons transferred for the respective oxidation process.

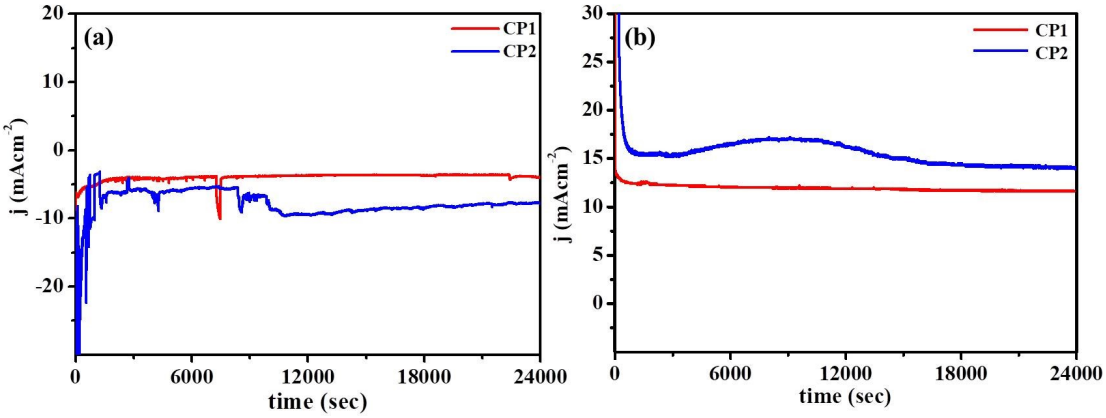

Fig. S16 (a) Chronoamperometric current stability of **CP1** and **CP2** for HER (b) Chronoamperometric current stability of **CP1/GCE** and **CP2/GCE** for OER.

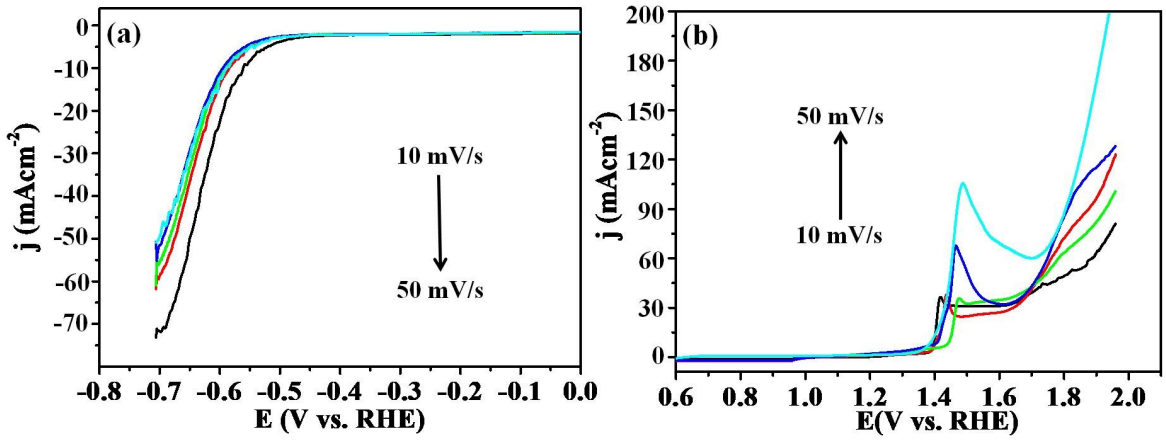

Fig. S17 (a) Electrochemical HER performance of **CP2** in H_2SO_4 at different scan rate 10 to 50 mV/s, (b) Electrochemical OER performance of **CP2** in KOH at different scan rate 10 to 50 mV/s.

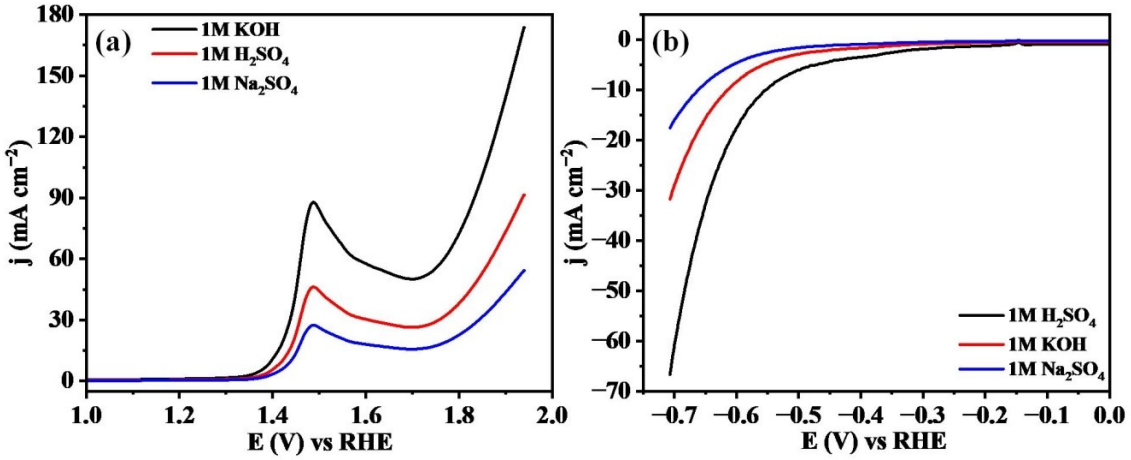

Fig. S18 (a) Electrochemical OER performance of **CP2** in 1M KOH, 1 M H_2SO_4, Na_2SO_4. (b) Electrochemical HER performance of **CP2** in 1M KOH, 1 M H_2SO_4 Na_2SO_4.

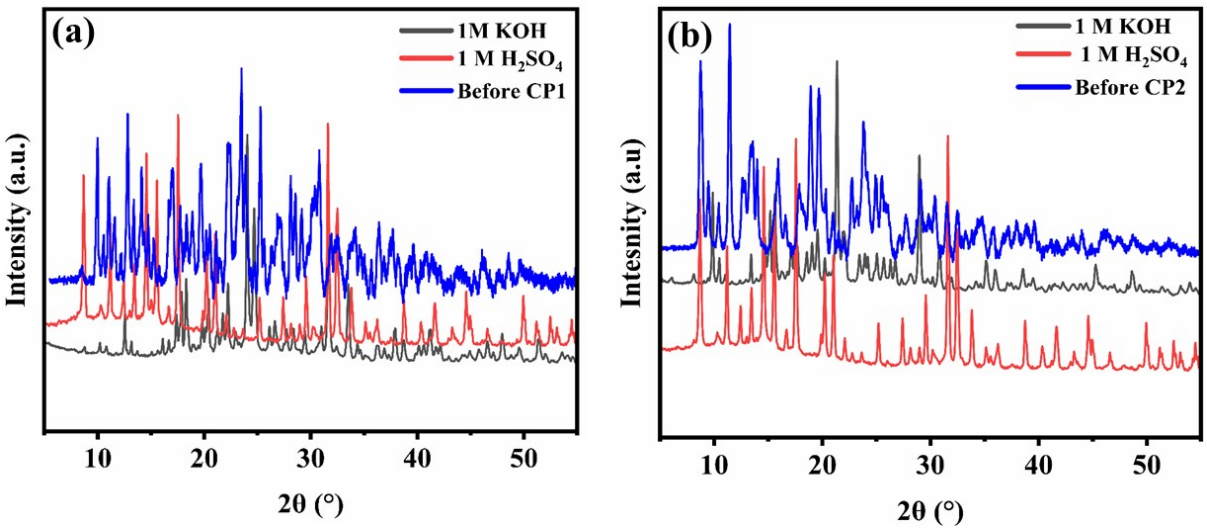

Fig. S19 PXRD images of (a) **CP1** and (b) **CP2** before and after soaking in 1.0 M KOH and 1.0 M H_2SO_4 for 12 h.

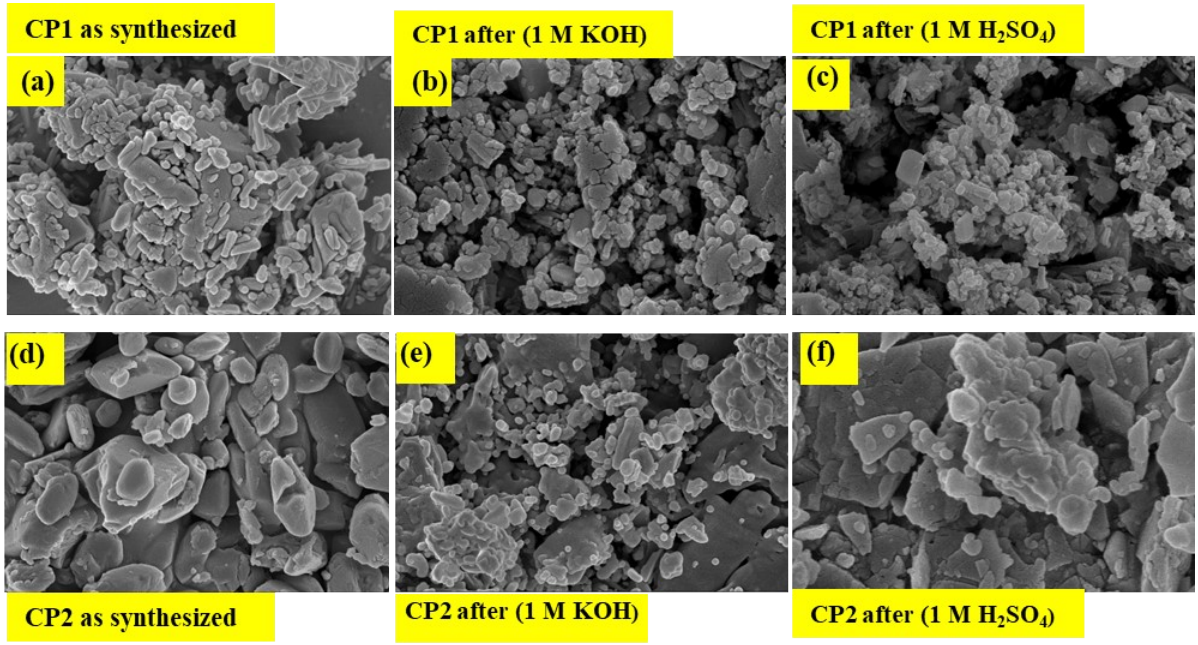

Fig. S20 SEM images of (a) **CP1** and (b) **CP2** before and after soaking in 1.0 M KOH and 1.0 M H_2SO_4 for 12 h.

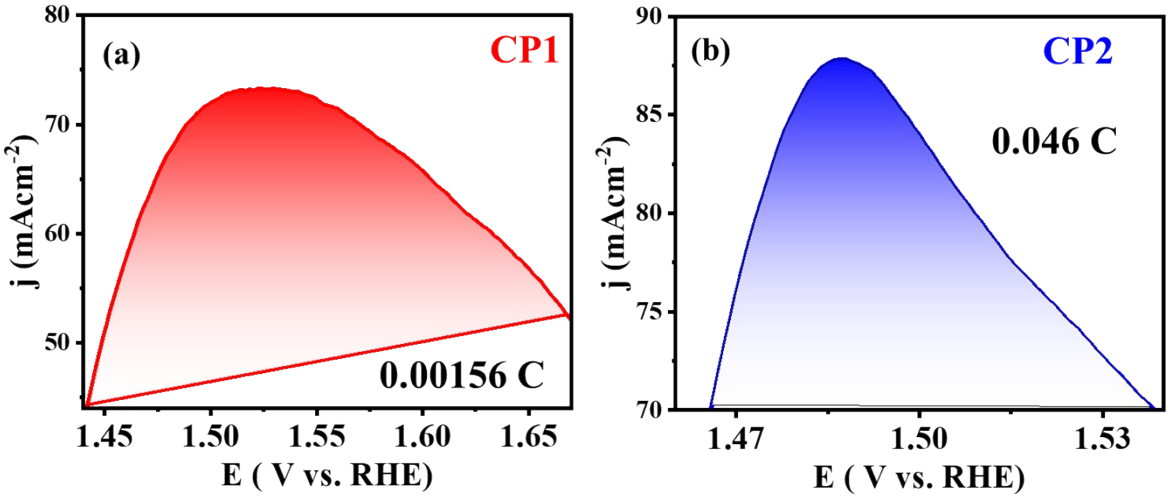

Fig. S21. Oxidation peak areas of **CP1** and **CP2** having charge 0.00156C and 0.046C respectively.

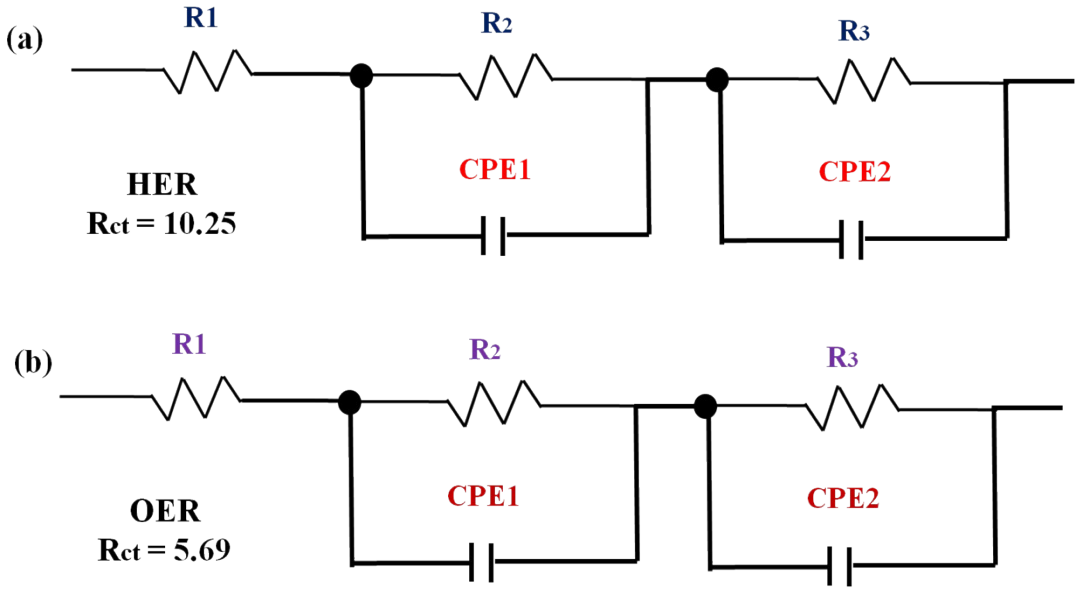

Fig. S22. Equivalent circuit of **CP2** consisting of a solution resistance (Rs), a charge-transfer resistance (Rct) with C_{dl} and Cps capacitance, and a constant-phase element (CPE). (a) The Rct value for **CP2** in H_2SO_4 (HER), (b) The Rct value for **CP2** in KOH (OER).

References:

S1. M. A. Spackman and D. Jayatilaka, *Cryst. Eng. Comm.,* 2009, **11**, 19.

S2. M. A. Spackman and J. J. McKinnon, *Cryst. Eng. Comm.,* 2002, **4**, 378.

S3. S. K. Wolff, D. J. Grimwood, J. J. McKinnon, M. J. Turner, D. Jayatilaka and M. A. Spackman, *Crystal Explorer 3.1*, University of Western Australia, 2012.

S4. APEX2, SADABS and SAINT, Bruker AXS Inc, Madison, WI, USA, 2008.

S5. S. Khullar and S. K. Mandal, *Cryst. Growth Des.,* 2013, **13**, 3116.

S6. G. M. Sheldrick, *Acta Crystallogr., Sect. C: Struct. Chem.,* 2015, **71**, 3.

S7. S. Khullar and S. K. Mandal, *Cryst. Growth Des.,* 2014, **14**, 6433.

S8. S. C. Dhawale, A. V. Munde, B. B. Mulik, R. P. Dighole, S. S. Zade and B. R. Sathe, *Langmuir.*, 2024, **40**, 2672.

S9. S. B. Roy, K. Akbar, J. H. Jeon, S. K. Jerng, L. Truong, K. Kim and S. H. Chun, *J. Mater. Chem. A.,* 2019, **7**, 20590.